Charles University in Prague
Faculty of Mathematics and Physics

BACHELOR THESIS

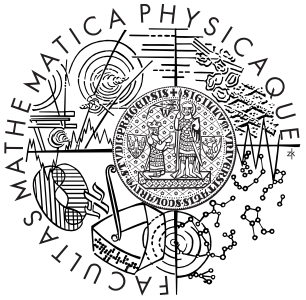

Miroslav Vácha

Measurement of runaway electrons in the CASTOR tokamak

Institute of Particle and Nuclear Physics

Supervisor: Mgr. Milan Krtička, Ph.D.
(Institute of Particle and Nuclear Physics)
Advisor: Mgr. Vladimír Weinzettl, Ph.D.
(Institute of Plasma Physics)
Study program: General Physics
2007

I am very grateful to my advisor Mgr. Vladimír Weinzettl, Ph.D. for his patient and careful guidance.

I declare that I have worked out this thesis by myself using only the literature cited here. I agree with lending of this thesis from the library of Faculty of Mathematics and Physics.

Prague, May 30, 2007 Miroslav Vácha

Preface

This thesis summarizes a part of results of the experimental campaign done on the CASTOR tokamak in October 2006, which was carried out by the team of scientists from The Andrzej Soltan Institute for Nuclear Studies (Poland) and The Institute of Plasma Physics AS CR, v.v.i.(Czech Republic).

The mentioned measurement was carried out as the P3 task of the research program supported by the EURATOM Community under the contract with the Association EURATOM-IPPLM, Poland. This research was also supported by the Ministry of Science and Higher Education, Poland, under contract No. 47/EURATOM/2005/7. The experiments on the CASTOR tokamak at IPP Prague were supported by the research grant No. AV0Z20430508.

Contents

Název práce: Měření ubíhajících elektronů na tokamaku CASTOR
Autor: Miroslav Vácha
Katedra (ústav): Ústav částicové a jaderné fyziky
Vedoucí bakalářské práce: Mgr. Milan Krtička, Ph.D.
e-mail vedoucího: krticka@ipnp.troja.mff.cuni.cz

Abstrakt: Práce shrnuje výsledky experimentálních měření rychlých elektronů s energií větší než 50 keV na tokamaku CASTOR, které byli provedeny pomocí nově navrženého Čerenkova detektoru. Prezentovány a diskutovány jsou změřené rozložení ubíhajících elektronů podél vedlejšího poloměru tokamaku při různých hustotách plazmatu a dále pak závislosti integrovaného čerenkovského signálu na hustotě plazmatu, proudu plazmatem a toroidálním magnetickém poli. V rámci práce byly rovněž analyzovány zdroje šumů čerenkovského signálu.

Klíčová slova: ubíhající elektrony, Čerenkovův detektor, tokamak

Title: Measurement of runaway electrons in the CASTOR tokamak
Author: Miroslav Vácha
Department: Institute of Particle and Nuclear Physics
Supervisor: Mgr. Milan Krtička, Ph.D.
Supervisor's e-mail address: krticka@ipnp.troja.mff.cuni.cz

Abstract: This thesis reports on results of the experimental measurements of fast electrons of energy higher than 50 keV on the CASTOR tokamak, which were performed using a new version of the Cherenkov detector. The measured radial distribution of the fast electron flux at different plasma densities and the dependences of the integrated Cherenkov signal on plasma density, discharge current, and toroidal magnetic field are presented and discussed. Possible sources of the noise on the Cherenkov signals are analyzed.

Keywords: runaway electrons, Cherenkov detector, tokamak

Chapter 1

Introduction

1.1 Thermonuclear fussion

A tokamak device is the most hopeful present concept realizing thermonuclear fusion of light atomic nuclei (Z $\sim$ 1) At high temperatures (T $> 10^6$K) and high densities of charged particles ($10^{18}m^{-3} < n < 10^{22}m^{-3}$), i.e. conditions suitable for carrying out fusion reactions, matter becomes a highly ionized plasma. Its electrically charged particles are confined inside a vacuum vessel of the tokamak by a strong magnetic field (B>1T).

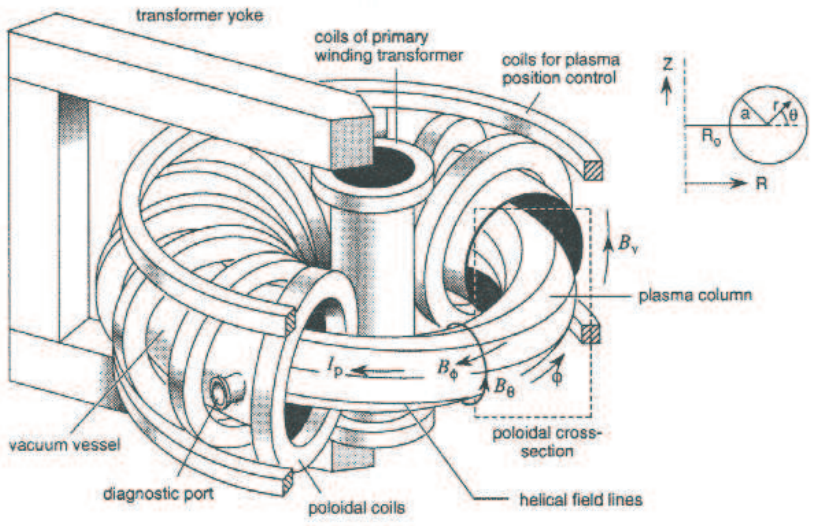

Figure 1.1: *Principal scheme of tokamak*

To ignite a thermonuclear synthesis it is necessary to put together fusing nuclei close enough to overcome strong repulsive electrostatic forces originating in an interaction between positively charged atomic nuclei. To pass these forces a thermal energy of chaotic movement of particles at extremely high temperatures can be used. Fusion reactions release by orders more energy than it is necessary for ignition. The main aim of the fusion research is a development of the thermonuclear reactor - a fusion power plant.

A principle of the tokamak device is relatively close to a collider, where charged particles are confined by a strong magnetic field in a vacuum vessel. In a collider, the number of particles is very low in order to prohibit interactions between them. Consequently, particle confinement is close to ideal and a single particle approximation describes a reality very well. On the other hand, in tokamaks and other fusion devices, a collective behaviour of charged particles plays a dominant role as a result of a high concentration (density) of charged particles. This state of matter is called plasma (for more details see [1]).

1.2 Fast electrons in tokamaks

A charged particle moving in fully ionized plasma is exposed to an electromagnetic influence of other particles and outer fields. Magnetic interactions between particles themselves can be neglected in plasma with low density. We will focus only at two-body coulombic collisions.

Thus characterized plasma can be described with Maxwellian velocity distribution.

$$f(u) = 4\pi \left(\frac{m}{4\pi kT}\right)^{3/2} u^2 exp\left[\frac{-mu^2}{2kT}\right] \tag{1.1}$$

In a simple approximation, it is possible to estimate influence of coulombic collisions on a charged particle motion with a frictional force:

$$F(u) = mu\nu \tag{1.2}$$

where m is mass of the charged particle, u its velocity and ν frequency of coulombic collisions. A detailed calculation of a mean frictional force effecting on electron in a Maxwellian plasma is shown in [2],[3] and [4].

Assuming an outer electric field in a direction of the electron velocity acts on this electron, the critical velocity uc can be defined as follows. An electron

has critical velocity, if his braking frictional force is equal to an influence of the accelerating outer field. An energy corresponding to critical velocity is called critical energy W_{crit}. Electrons moving along outer electric field lines with a velocity higher than critical are permanently accelerated by this field. They are called runaway electrons. The rest of electrons, i.e. electrons with energies lower than critical, stays in the Maxwellian distribution thanks to sufficiently frequent collisions.

Critical energy W_{crit} can be derived using a friction force (see [2], [4]):

$$F_e = eE_c \frac{2kT_e}{m_e u_0^2} \tag{1.3}$$

$$F_i = Z_{eff} eE_c \frac{kT_e}{m_e u_0^2} \tag{1.4}$$

where E_c is critical electric field

$$E_c = \frac{e^3 n_3 ln\Lambda}{8\pi\epsilon_0^2 m u_0^2} \tag{1.5}$$

and Z_{eff} is effective charge of plasma particles

$$Z_{eff} = \frac{\sum N_i Z_i^2}{n_e} \tag{1.6}$$

where N_i is a density of Z_i times ionized atoms and n_e is an electron density.

The resulting equation of motion for the test electron is

$$e\left[E - E_c\left(1 + \frac{Z_{eff}}{2}\right)\frac{kT_e}{W_{crit}}\right] = 0 \tag{1.7}$$

where E is an external electric field accelerating the electrons in the toroidal direction. The inferred critical energy can be expressed as

$$W_{crit} = \frac{E_c}{E}\left(1 + \frac{Z_{eff}}{2}\right) kT_e \tag{1.8}$$

In tokamak plasma, an essential part of runaway electrons originates from the first moments of the discharge due to a high intensity of the electric field in breakdown phase. Moreover, a cross-section of coulombic collisions is lower in partially ionized plasma than in fully ionized one for energies lower than 70eV. It means that critical energy is lower until plasma is fully ionized. At the beginning of discharge those two effects cause a short-term high rapidity of the runaway electrons generation (more in [5] and [6]).

1.3 Cherenkov radiation

The Cherenkov radiation is an electromagnetic radiation emitted when a charged particle passes through an insulator with a speed greater than the speed of light in that medium. That means the refractive index of this medium is greater than 1. As a charged particle goes through, it disturbs the local electromagnetic field in that medium. Electrons of atoms in the medium are displaced and polarized by the electromagnetic field of the charged particle. Than photons are emitted when the insulator's electrons restore themselves to an equilibrium. In a conductor, the electromagnetic field disturbance can be restored without emitting a photon. As the particles slow down to the local speed of light, they produce a cone of the Cherenkov radiation (see Fig.1.2).

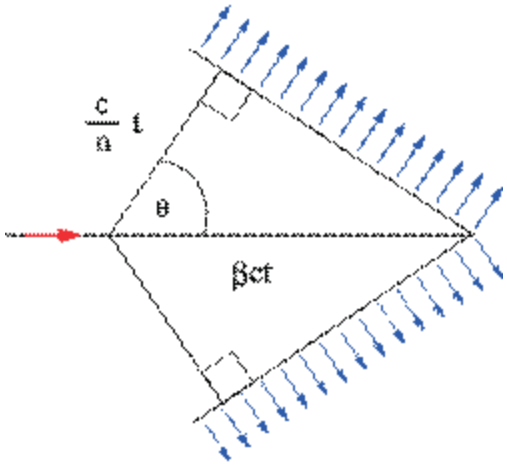

Figure 1.2: *The geometry of the Cherenkov radiation generation. The particle with the velocity v (red arrow), β is v/c, θ is the refractive index of the medium. The blue arrows are photons.*

The emision angle θ of Cherenkov radiation photons can be simple calculated from the formula:

$$cos\theta = \frac{1}{n\beta} \tag{1.9}$$

The overall intensity of Cherenkov radiation is proportional to the velocity of the passing particle and to the number of such particles. Unlike

emission spectra, which have spectral peaks, Cherenkov radiation is continuous. The total amount of energy radiated per unit length is:

$$\frac{dE}{dx} = \frac{q^2}{4\pi} \int_{v>c/n(\omega)} \mu(\omega)\omega \left(1 - \frac{c^2}{v^2 n(\omega)^2}\right) d\omega \tag{1.10}$$

where μ is the permeability, $n(\omega)$ index of refraction of the medium, q is the electric charge of the particle, v is the speed of the particle, c is the speed of light in vacuum, and ω is the angular frequency of radiation.

Cherenkov radiation is often used in experimental particle physics for a particle identification. One could measure a velocity of the electrically charged elementary particle by the properties of the Cherenkov light emitted in a medium. If the momentum of the particle is measured independently, one could compute the mass of the particle. In tokamak experiments Cherenkov radiation is commonly used for a fast electrons presence identification, namely as a consequence of ohmic or auxiliary plasma heating (more details in [4]).

1.4 Motivation

An investigation of the fast particles generation and their behavior in high-temperature plasma is important for the construction of big tokamaks and future fusion reactors in general. These particles diffusing across the magnetic field lines outward a hot plasma core may cause a significant damage of the first wall components. This can bring next undesirable financial expenses.

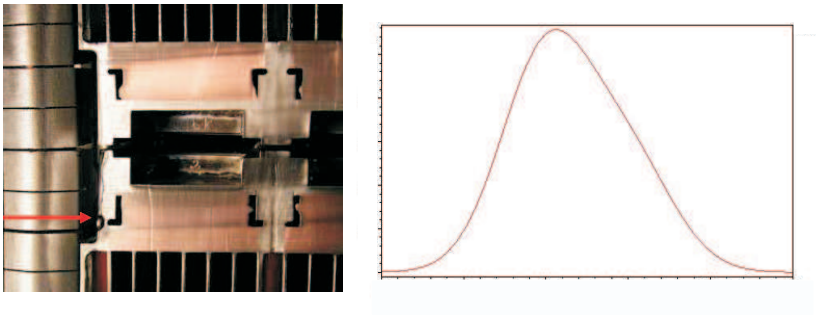

Figure 1.3: *Damage of first wall (left), disturbed maxwelian distribution (right)*

A next reason of the runaway electrons research is that they can significantly affect results of the measurement, due to the fact that they do not yield the maxwellian distribution, while interpretations of e.g. probe measurements are based on it (more in [7], [9] and [10]).

On the other hand runaway electrons have also a positive meaning. They can be used to probe a magnetic turbulence in core of plasma. That's because their confinement depends on the magnetic field turbulence, when they are nearly collisionless (for more details see [6]).

Chapter 2

Measurement

2.1 Tokamak CASTOR

The CASTOR (Czech Academy of Sciences TORus) experiment, which was operated at the Institute of Plasma Physics in Prague until 2006, is one of the smallest and oldest tokamak in the world. It is a reconstructed version of the originally Russian TM-1 tokamak.

Major radius	R = 0.4m
Minor radius (wall)	a_{wall} = 10cm
Minor radius (limiter)	a = 6cm or a = 8.5cm
Discharge time	t < 50ms
Toroidal magnetic field	0.5T < B_T < 1.5T
Plasma current	5kA < I_p < 17kA
Plasma density	$4.10^{18}m^{-3} < n_e < 2.10^{19}m^{-3}$
Electron temperature	$T_e(0) < 300$eV
Ion temperature	$T_i(0) \sim 100$eV

Table 2.1: *Main parameters of the CASTOR tokamak*

CASTOR, thanks to its parameters, is counted in the class of so-called "small tokamaks" with a low central temperature of plasma causing almost no thermonuclear reactions. This sort of tokamaks is used mainly to investigate an edge plasma region, to develope and test new plasma diagnostics and to realize various experiments thanks to their flexibility.

CASTOR is a limiter tokamak with a circular profile of plasma. A removable limiter is composed of a part of the poloidal ring made from molyb-

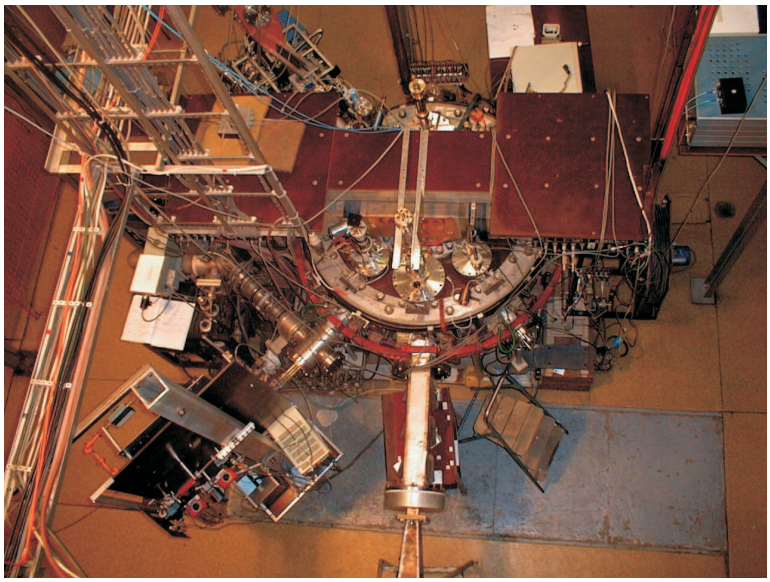

Figure 2.1: CASTOR tokamak

denum (inner radius 8.5cm or 6cm). A tokamak toroidal vacuum chamber consists of a welded segment of stainless steel bellows. The chamber is a secondary winding of the transformer, what has a two arms closed iron core. The length of discharge on CASTOR is limited by a capability to generate a strong toroidal magnetic field for a plasma insulation from the material wall. A toroidal magnetic field is generated by 28 coils connected in series. They are powered by condenser batteries. Maximal toroidal magnetic field is 1.5T. To reach a sufficient plasma confinement it is necessary to generate at least 0.5T. Consequently, the discharge time is limited by 50ms. A working gas in the CASTOR tokamak is hydrogen (light isotope ^1H). Technical hydrogen is purified by atomic diffusion through heated palladium or nickel electrodes. A purity of used hydrogen is critical, because of only few percents of impurities can evoke a disruption of the discharge or even can cool down a plasma by a strong radiation. A working pressure of hydrogen before the discharge is about 10^{-2}Pa. During the discharge it is possilbe a pulse gas puffing trough a fast piezoelectric valve. A purity of the tokamak chamber is provided by rotary and turbo-molecular pumps up to pressure 10^{-4}Pa. Next methods are a glow discharge and a baking, which is used mainly after an opening of the chamber. At temperatures 200-300°C an outgassing is done(for more details see [14]).

2.2 High-temperature dicharges of the CASTOR tokamak

A standard shot of the CASTOR tokamak is a hydrogen high-temperature discharge with the plasma current Ip∼8-10kA, the line-integrated electron density n_e∼7-10*$10^{18}m^{-3}$, the magnetic field B_T ∼1.3T and with the discharge duration τ=25-30ms.

A stationary phase of the discharge begins typically 5ms after the breakdown. It features nearly time-independent properties of the plasma that it is possible to describe it by constant values of the main plasma parameters such as loop voltage U_{loop}, plasma current I_p, electron density n_e, toroidal magnetic field B_T and electron temperature T_e.

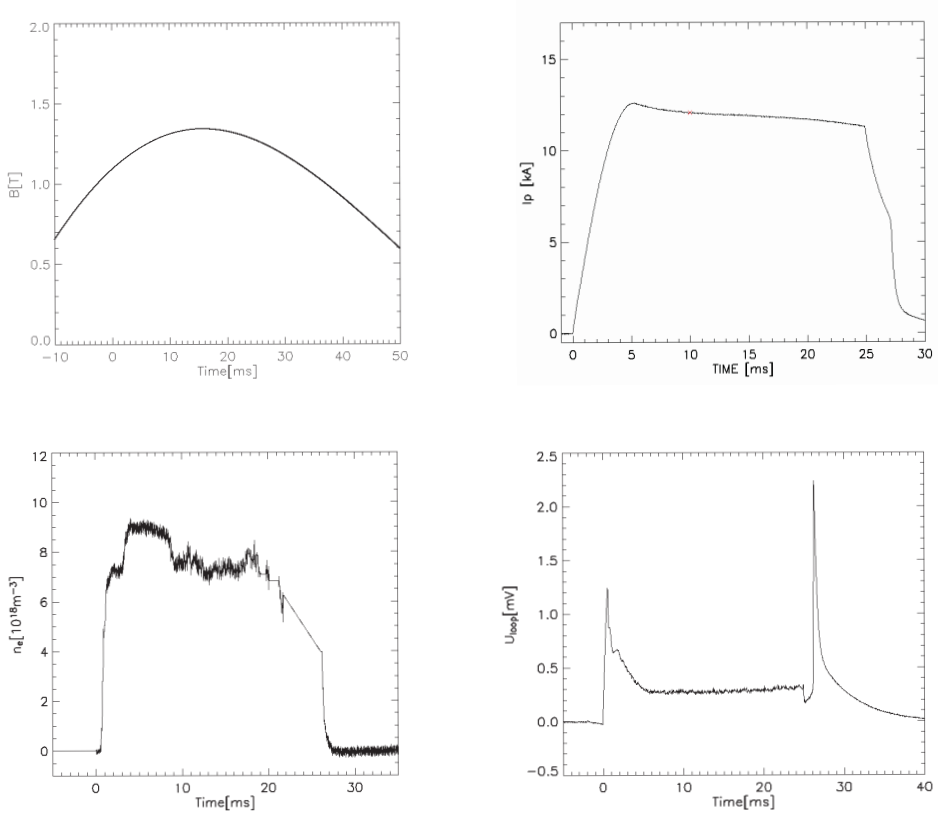

Figure 2.2: *Typical discharge parameters of the CASTOR tokamak. Toroidal magnetic field, plasma current, electron density and loop voltage.*

High temperature discharges on the CASTOR tokamak can be different in length 5ms $\leq \tau \leq$ 50ms, magnitude of the toroidal magnetic field 0.5T$\leq B_T \leq$1.5T, amount of puffed hydrogen (stationary chamber filling and impulse puffing). The electron temperature T_e ∼150-300eV together with the plasma current, in the range of 5kA $\leq I_p \leq$ 17kA, can be changed via the different ohmic input power (more in [14]).

2.3 Cherenkov detector

A design of the detector was developed according to a principle mentioned in above; when a charged particle is passing trought an insulator with a refraction index greater than 1 and the particle velocity is higher than the velocity of light in this medium, the Cherenkov radiation is emitted. Employed detector contains the detection head with Cherenkov radiator, in which Cherenkov radiation is emitted, and a photomultiplier joined to the head with optical fibres.

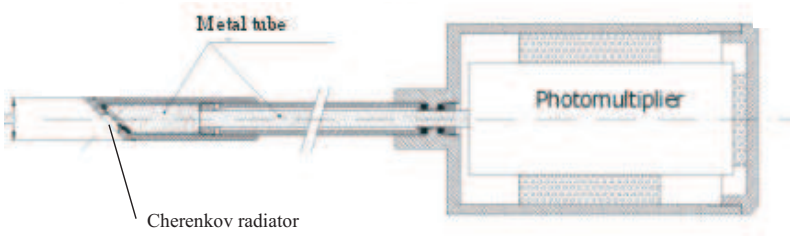

Figure 2.3: *Ilustrative scheme of the Chrenekov detector*

The detection head consists of the Cherenkov-type radiator made of the aluminium nitride (AlN) crystal (the effective diameter 5mm), which was coated with a 10μm Ti layer. This configuration allows recording of electrons with energy higher than 50keV. After the quartz light-pipe was replaced by a thin metal tube with polished inner walls, all detrimental scintillations (which might be induced inside the quartz) have completely been eliminated. The detector is connected with a fast photomultiplier through an optical cable of 10m in length. Cherenkov signals are recorded by this photomultiplier (for more details see [12] [13]).

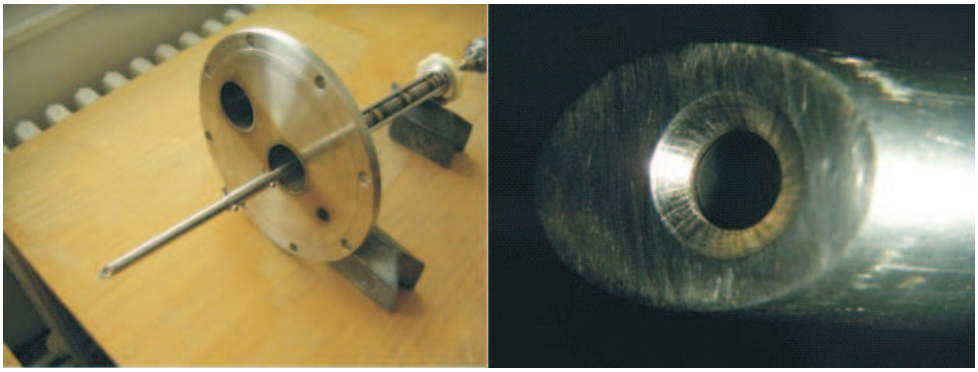

Figure 2.4: *Head of the Cherenkov detector placed on the movable support on the flange of the diagnostic port (left). A detail showing an entrance window of the detection system (right).*

2.4 Measurement

2.4.1 Experimental setup

The Cherenkov detector was placed on the vertically movable support and instaled into the upper diagnostic port at an angle 45° toroidally from the limiter. It allows measurement in radial positions from 60mm (a confined

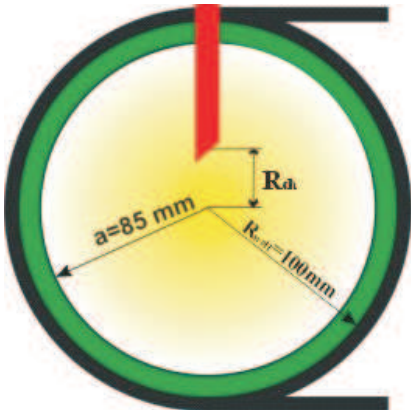

Figure 2.5: *Scheme of the detector insertion inside tokamak: a red color indicates the detection head, a region of the limiter shadow is green, vacuum vessel walls are black.*

plasma region) up to 100mm (a diagnostic port shadow). Local hard X-rays

of energy within the range from 20 to 200keV originating in a close vicinity of the Cherenkov head were monitored using a plastic scintillator equipped with a copper filter. The described detectors were connected with fast photomultipliers through optical cables of 10m in length. The photomultipliers recording both signals were hidden inside a lead shielding (pill-box) with walls of about 15cm in thickness. An output voltage (U_{ch}) of the 'Cherenkov' photomultiplier is proportional to the fast electron streams reaching the Cherenkov radiator and is used and processed in the next calculations in the following sections.

On the CASTOR tokamak, the experimental data were collected in 462 shots performed with the ohmic heating (OH mode), with the discharge time $\tau = 25$ms, the discharge current 5 kA $\leq I_P \leq$ 15kA, and the toroidal magnetic field 0.8 T $\leq B_T \leq$ 1.5 T. Described measurements were carried out at a relatively low plasma density (n_e= 0.5-1.5*$10^{19} m^{-3}$), but at a relatively high acceleration voltage (2.0V $\leq U_{loop} \leq$ 4.0V).

2.4.2 Typical discharge data

The typical CASTOR discharge in the Cherenkov campaign was 25ms long. It can be divided into three parts: breakdown or starting phase, stacionary phase and ending or shortage phase. In Fig. 2.6 a temporal evolution of the most important plasma parameters is shown: plasma density n_e, loop voltage U_{loop}, plasma current I_p, Cherenkov detector signal, H_α radiation and hard X-ray signals. Main plasma parameters are nearly constant in the stacionary phase with an accuracy about 5%.

The different radiation detectors present on the CASTOR tokamak are not absolutely calibrated, therefore an intensity of the measured signals is usually yielded in arbitrary units. It should be noticed it typicaly represents output voltages from appopriate photomultipliers.

A behavior of the Cherenkov signal can be described as a typically ascending function with many sharp peaks. Hence, the signal can be used as an integral value over the desired time interval or statisticaly processed as sequence of independent peaks.

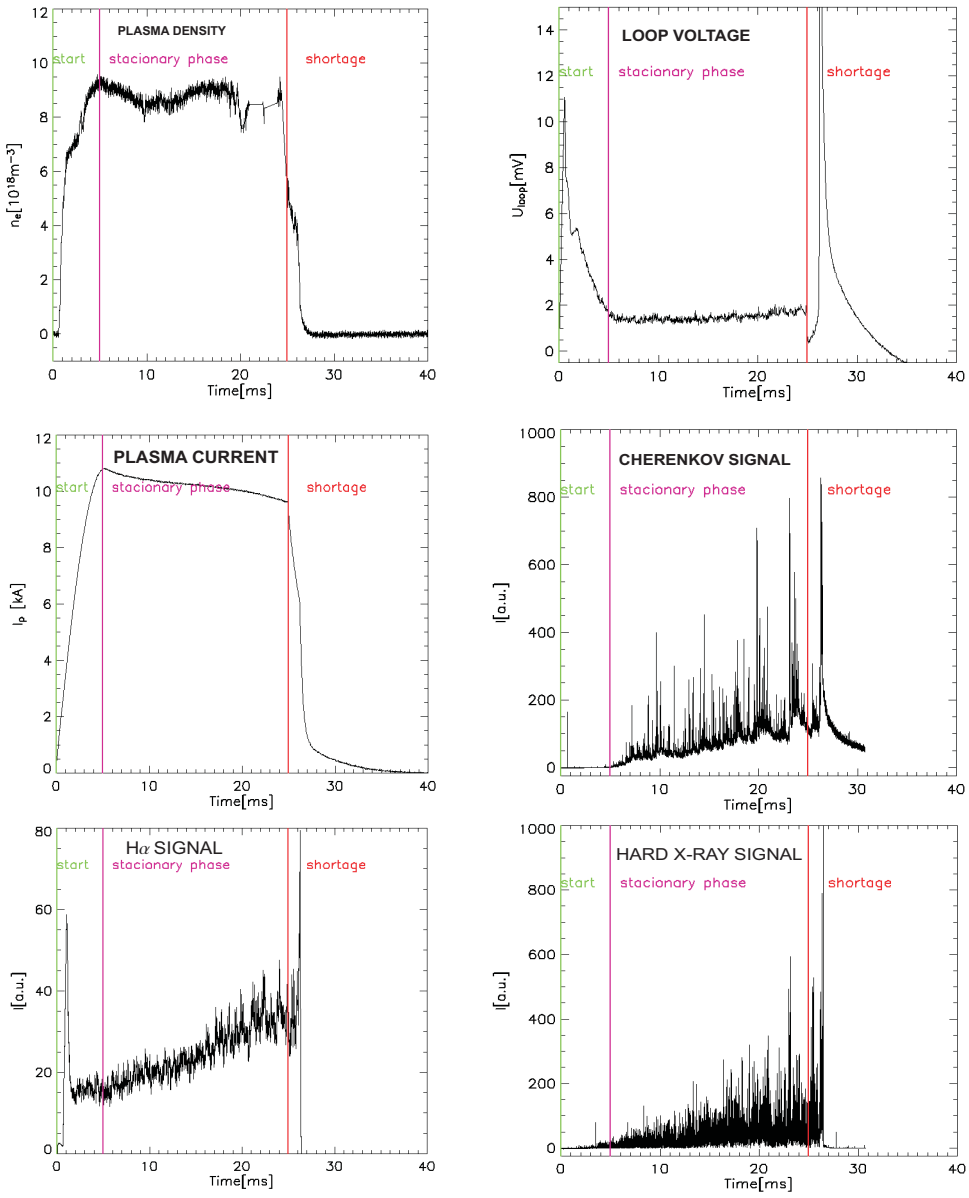

Figure 2.6: Typical data obtained from the measurement: plasma density, loop voltage, plasma current and Cherenkov, H_α and hard X-ray signals

2.4.3 Raw signal and its corrections

Cherenkov data were collected by the fast data acquisition computer from t_0=-2ms (2ms before the shot) with 1ms sampling. The total number of samples was 32768, what covers the whole period of the tokamak discharge.

The first two milliseconds of the data were used for zero level estimation. It was calculated as weighted average of the two most frequent values in a signal instead of its main value. The idea of this procedure was to take away high random looming peaks, which can distort the main value.

It was also found that certain undershoot is present in a signal during first milliseconds of the shot (data points in orange rectangle in Fig.2.7). This signal behavior is given by fast electromagnetic changes close to breakdown phase of the discharge and cannot be simply dispatched. Consequently, only data from 5ms to 25ms were considered.

To prove whether the measuring circuit is well protected against electromagnetic interferences and the secondary radiation (e.g. Bremsstrahlung from the detector head shielding), the entrance window of the detector, by default oriented in the direction opposite to the plasma current allowing fast electron measurements, was turned around its axis by 180 degrees in agreement with the plasma current in some shots of the campaign. The recorded signals were in this case very low (practically negligible) as will be shown later.

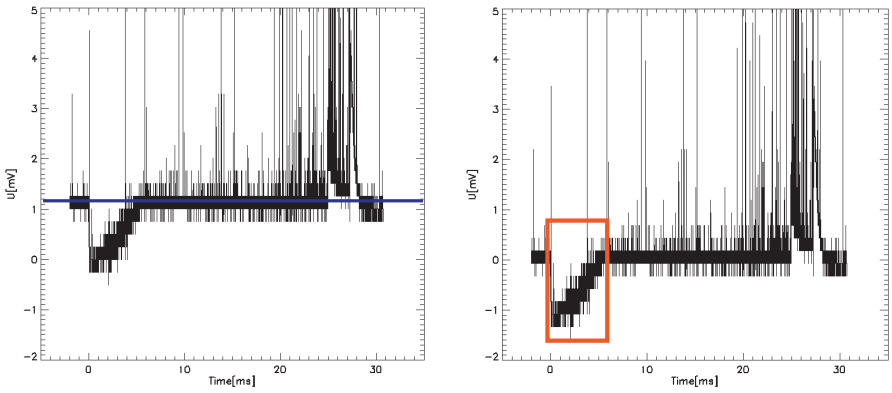

Figure 2.7: *Zero level estimation is shown on a raw data (left). Data with a signal undershoot at the beginning of the discharge are excluded from the next data processing.*

2.5 Photomultiplier Shielding

2.5.1 introduction

The first shots indicated the need to shield both the photomultipliers (for Cherenkov and hard X-Ray radiation detection) which are very sensitive to a direct radiation from the tokamak. Thus, the photomultipliers were moved into the room neighbour to tokamak hall (∼10m far from the tokamak). A bunker (Fig. 2.8) consisting of lead brick walls was built around them.

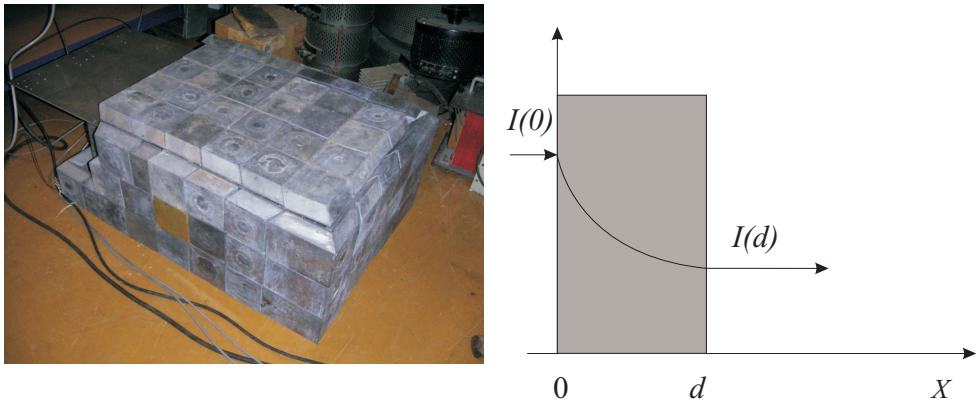

Figure 2.8: Lead bunker (left), radiation attenuation in a material wall (right)

Radiation attenuation in a material wall is descibed by the well-known formula 2.1 and is shown in Fig. 2.8 (for more details see [15])

$$I = I_0 exp(-\mu x) \tag{2.1}$$

Each lead brick of width Δ_B=5 cm decreased the background level by one order. An acceptable background level was reached for the three walls bunker.

2.5.2 Direct Radiation Background

A direct radiation passing through the detector shielding can significantly increase a noise level of the measured signal. In general, the direct radiation has a wide energy spectrum and cannot be easily handled. However, in the case of the high-energy decaying tail of the tokamak spectrum, a raw estimation of the dominant contribution and its influence on the measured signal

will be sufficient. Therefore, the next constructions will be done assuming only a monoenergetic direct radiation background. A validity of this aproach and conditions, where it can be used, will be discussed in chapter 3.

An estimation of the direct radiation background and its energy was done in the shots, where the lead brick wall bunker was removed stepwise. A numerical integral ($\Sigma U_{ch}t$) of the detected radiation over the shot period of 5-25ms was calculated for the unshielded and shielded (by 1, 2 and 3 lead bricks) photomultiplier, see Table 2.2

Δ_B [number of bricks]	Number of shots (shot numbers)	$\Sigma U_{ch}t$ [V. ms]	σ [V.ms]
0	3 (#270,271,272)	530.3	24
1	4 (#263,264,265,266)	49.4	3.7
2	6 (#257,258,259,260,261,262)	5.5	0.7
3	5 (#252,253,254,255,256)	1.5	0.5

Table 2.2: *Direct radiation background - lead shielding*

The measured dependence was fitted according to formula 2.1 extended by a term U_B corresponding to other sources of radiation background (cosmic rays, detector noise, etc.) using formula 2.2

$$Y = U_{ch0}exp(-\mu_B x_B) + U_B \tag{2.2}$$

where $U_{ch0} + U_B$ is a radiation detected by an unshielded detector, μ_B is attenuation factor in units of led brick shielding. The fitted dependence with the following parameters is shown in Fig. 2.9

$U_{ch0} = 529.3V\mu.s$

$\mu_B = 2.39brick^{-1}$

$U_B = 1.1V.\mu s$

To calculate standard attenuation factor μ, the parameter μ_B must be divided by the brick width ΔB:

$$\mu = \frac{\mu_B}{\Delta_B} \tag{2.3}$$

The resulted attenuation factor is $\mu = (0.478 \pm 0.005)cm^{-1}$ and a corresponding value for a comparison with the Tables [16] is $\mu/\rho = (42,2 \pm 0,5) * 10^{-3}cm^2/g$ (for r = 11,34 g/cm^3).

Because of all measurements were carried out by the three lead bricks shielding, hereafter, the value of direct radiation for three lead brick shielding

$\Sigma U_{ch}t$=1.5V.ms obtained from fit with formula 2.2, will be used as a value of direct radiation background.

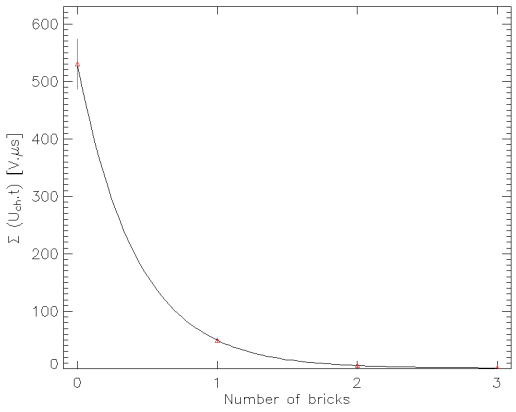

Figure 2.9: *Attenuation of direct radiation detected by a photomultiplier by the lead brick bunker.*

Polynomial fit of values from [16] was intersected with obtained factor μ/ρ (Fig. 2.10). This procerude gave energy range E=(3.9±1.0)MeV.

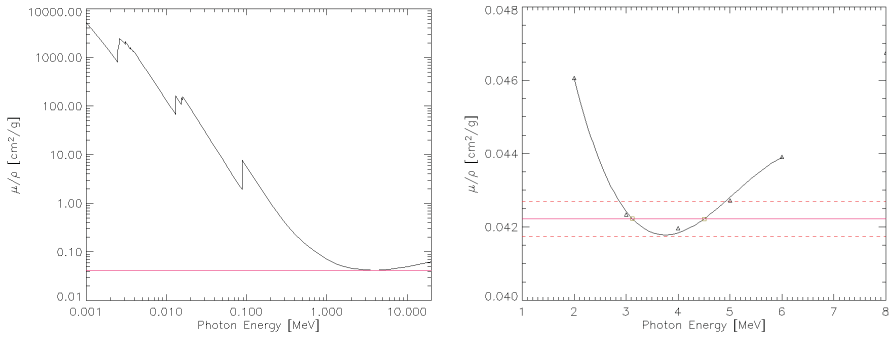

Figure 2.10: *Dependence of attenuation factor of lead on photon energy and its comparison with the measured value of attenuation factor (left). The detail of MeV range is shown on the right graph*

Similar procedure as described above was done using a water shielding. An integral of the detected radiation over the shot period of 5-25ms was calculated for a photomultiplier shielded by both one brick of lead and

Δ_B [number of bricks]	Number of shots (shot numbers)	$\Sigma U_{ch}t$ [V. ms]	σ [V.ms]
one lead brick and bottle of water	3 (#267,268,269)	20.2	0.7

Table 2.3: *Direct radiation background - water shielding*

a bottle of watter (diameter 27cm), see Table 2.3 The measured atenuation in water corresponding to formula 2.1 was fitted using equation 2.2 with U_{ch0}=49.4 and U_B=1.1 obtained as fit parameter from shielding measurements with lead bricks. The fitted dependence with the fit parameter

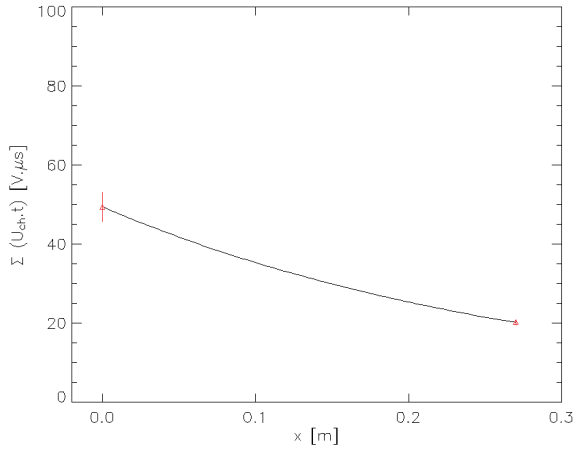

Figure 2.11: *Attenuation of direct radiation detected by a photomultiplier by the bottle of water shielding.*

μ_B=3.46 is shown in Fig.2.11 The value for a comparison with the Tables [16] is μ/ρ=(34.7±0.1)*10^{-3} cm^2/g (for ρ=0.998g/cm^3 at 20±1°C). A precision of μ/ρ determination originates in temperature dependence of water density.

Polynomial fit of values from [16] was intersected with obtained factor μ/ρ (Fig. 2.6.). This procedure gave value of energy E=(3.8±0.1)MeV.

Assuming a dominating energy range in direct radiation, the resulted energy for lead shielding was estimated as E=(3.9±10)MeV, what gives the same energy as for water shielding E=(3.8±0.1)MeV. Although it is clear that real radiation spectrum from the tokamak is very wide, the inferred

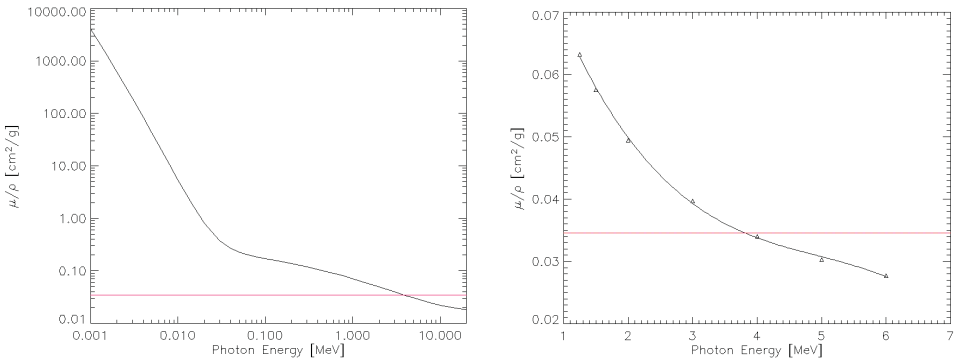

Figure 2.12: *Dependence of attenuation factor on photon energy and its comparison with the measured value of attenuation factor (left). The detail of MeV range is shown on the right graph.*

estimation of dominating energy in direct radiation background is still valid as a consequence of the form of attenuation factor dependence on energy for lead. Moreover, this deduction is strengthened by the same result for a water shielding, while the form of attenuation factor dependence on energy for water is different than for lead.

2.6 Experimental results

In the following, a radial distribution of fast electrons and dependences of the integrated Cherenkov signal on various plasma parameters are reported. The plots show the time-integrated values (over time interval from 5 to 25ms) of the Cherenkov signals proportional to the fast electron streams reaching the detector.

The distribution of the fast electron fluence as a function of the minor radius R_{ch} was measured in the edge plasma region. A position of the Cherenkov head was changed from a shadow of the diagnostic port (R_{ch} >100mm) up to a confined plasma region (R_{ch} ∼60mm; limiter radius R_L=85mm). It should be noticed that the horizontal detector position is stable and set to major radius of the tokamak R=40cm. There were carried out three measurements. Two at the medium plasma density and one at low plasma density. The results are shown in tables 2.4, 2.5 and 2.6. The measured dependences are also shown in figures 2.13 and 2.14. A comparison

of the measurements at two different values of the plasma density are shown in Fig. 2.14. In this figure a comparison with the ion side measurement is shown too. Other parameters were kept to be constant at standard values: I_p=10-11kA, B_T ~1.3-1.4T.

R_{ch} [mm]	Number of shots (shot numbers)	$\Sigma U_{ch}t$ [V. ms]	σ [V.ms]
60	2 (#24,25)	3314.9	191.0
65	2 (#26,27)	1755.2	22.2
70	2 (#28,29)	585.5	157.5
75	2 (#30,31)	105.0	38.7
80	2 (#32,33)	30.2	0.7
85	2 (#34,35)	18.6	0.5
90	2 (#36,37)	17.0	0.6
95	2 (#38,39)	14.4	0.5
100	2 (#40,41)	13.9	0.5

Table 2.4: *Position scan medium density - electron side; shots #24-41*

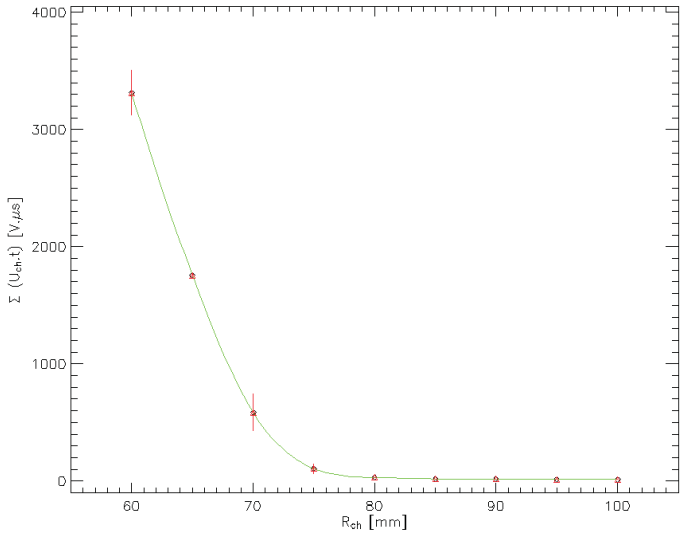

Figure 2.13: *Dependence of the electron fluence on the position of the Cherenkov detector along the CASTOR minor radius at medium plasma density (1.2*10$^{19}m^{-3}$).*

R_{ch} [mm]	Number of shots (shot numbers)	$\Sigma U_{ch}t$ [V. ms]	σ [V.ms]
60	2 (#32740,32741)	3751.5	368.5
65	4 (#32738,32739,32742,32743)	1398.9	189.3
70	4 (#32736,32737,32744,32745)	636.0	221.9
75	4 (#32734,32735,32746,32747)	221.4	63.5
80	2 (#32748,32749)	74.1	4.4
85	2 (#32750,32751)	32.3	3.9
90	2 (#32752,32753)	23.9	1.8
95	2 (#32754,32755)	17.9	1.0
100	2 (#32756,32757)	16.6	0.5

Table 2.5: *Position scan at low plasma density - electron side; shots #32734-32757*

R_{ch} [mm]	Number of shots (shot numbers)	$\Sigma U_{ch}t$ [V. ms]	σ [V.ms]
60	2 (#86,87)	1563.4	123.6
65	2 (#97,98)	607.4	50.2
70	2 (#99,100)	145.3	27.3
75	2 (#109,110)	20.0	2.8
80	2 (#111,112)	10.5	0.5
85	2 (#122,123)	11.5	0.6
90	2 (#124,125)	10.7	0.6
95	2 (#134,135)	8.30	0.5

Table 2.6: *Position scan at medium plasma density - electron side, shots #86-135*

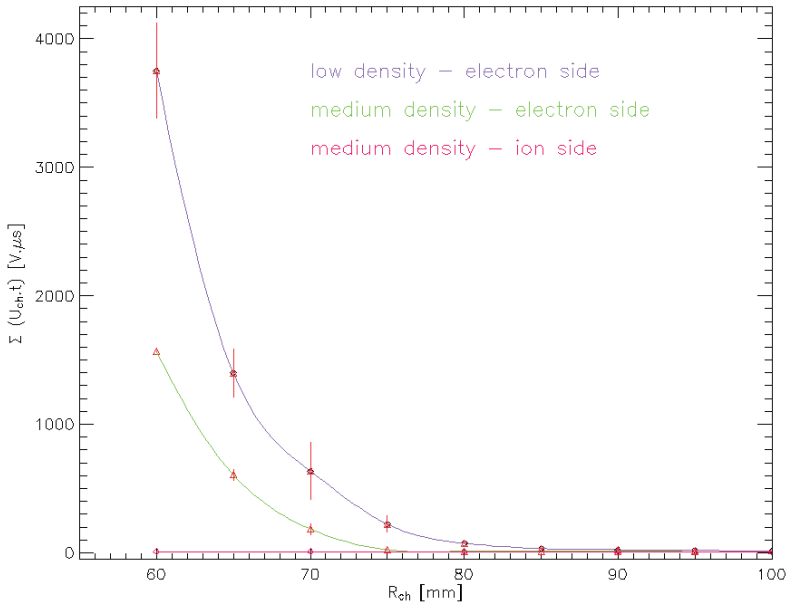

Figure 2.14: *Comparison of dependences of the electron fluence on the position of the Cherenkov detector along the CASTOR minor radius at low plasma density (6.5*$10^{18}m^{-3}$) -the purple curve, at medium density (1.2*$10^{19}m^{-3}$) - the green curve and for the ion side measurement - the red curve.*

The density effect is clearly demonstrated in the next tokamak shots at the fixed detector position (R_{ch}=70mm) and at various plasma densities. The plasma density was regulated by a puffing of an additional amount of the working gas (hydrogen). Experimental results are shown in table 2.7. The measured dependence and a comparison with the results of the measurement with an opposite head orientation. are shown in figure 2.15.

Magnitude of the Cherenkov emission also depends on the plasma current, therefore measurements at different values of plasma current were carried out. The detector position R_{ch} was 70mm and the magnetic field B_T=1.3T. The results are exposed in table 2.8. The dependence is yielded in Fig. 2.16. A big scatter of the measured points is probably hidden in other plasma parameters like plasma density, which, unfortunately, cannot be kept constant simultaneously with the plasma current changes on the CASTOR tokamak.

Density $[10^{18}m^{-3}]$	Number of shots (shot numbers)	$\Sigma U_{ch}t$ [V. ms]	Density $[10^{18}m^{-3}]$	Number of shots (shot numbers)	$\Sigma U_{ch}t$ [V. ms]
8.6	1 (# 143)	42.4	14.7	1 (# 156)	608
8.5	1 (# 144)	43.7	11.3	1 (# 157)	46.8
8.9	1 (# 145)	25.9	10.6	1 (# 158)	27.3
9.1	1 (# 146)	40.8	9.3	1 (# 159)	29.2
9.7	1 (# 147)	24.6	8.2	1 (# 160)	103.6
9.9	1 (# 148)	39.6	8.1	1 (# 161)	133.5
11.3	1 (# 149)	59.9	6.9	1 (# 162)	359.8
11.5	1 (# 150)	39.7	7.1	1 (# 163)	366.0
11.2	1 (# 151)	56.3	5.7	1 (# 164)	1389.2
11.8	1 (# 152)	42.4	5.8	1 (# 165)	1144.2
12.4	1 (# 153)	84.8	5.5	1 (# 166)	1265.6
12.8	1 (# 154)	68.4	5.4	1 (# 167)	1245.7
13.8	1 (# 155)	179.2	-	-	-

Table 2.7: *Line average density scan- electron side; shots #143-167*

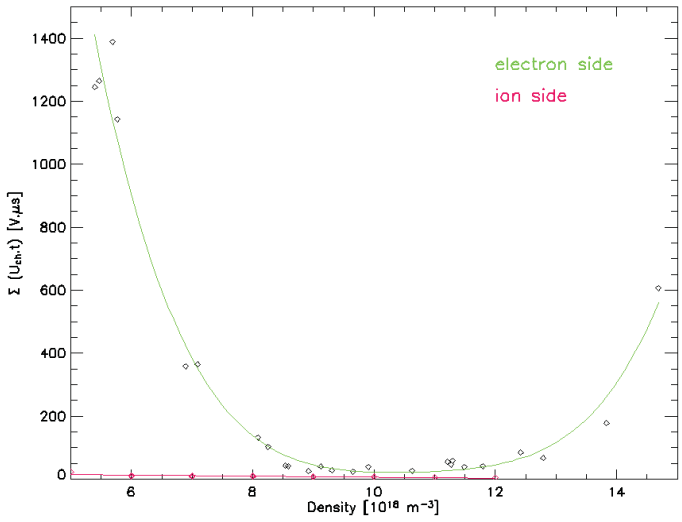

Figure 2.15: *Integrated Cherenkov emission as a function of the plasma density. The green curve represents an orientation of the detection head allowing fast electron measurements, the purple curve shows a comparison with ion side measurements.*

I_P [kA]	Number of shots (shot numbers)	$\Sigma U_{ch}t$ [V. ms]
7.32	1 (#46)	649.1
8.77	1 (#47)	1544.2
10.49	1 (#48)	486.8
10.50	1 (#49)	860.4
12.07	1 (#50)	1207.2
13.43	1 (#51)	2224.0
13.77	1 (#52)	1093.5
15.13	1 (#53)	2489.60

Table 2.8: *Plasma urrent scan- electron side; shots #46-53*

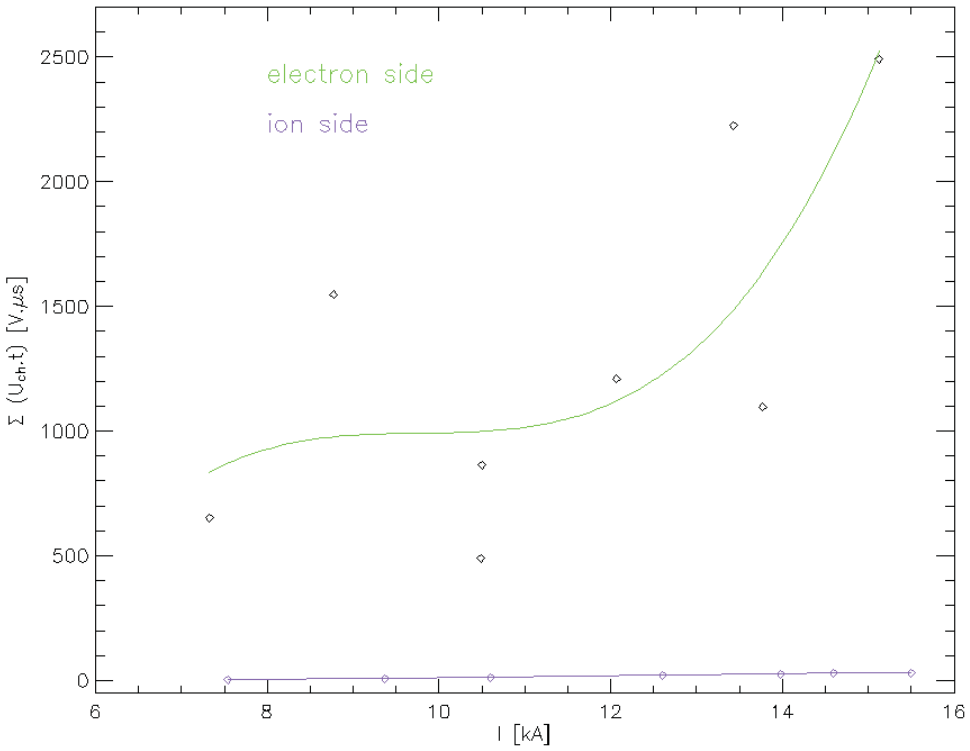

Figure 2.16: *Integrated Cherenkov emission as a function of the plasma current. The green curve represents an orientation of the detection head allowing fast electron measurements, the purple curve shows a comparison with ion side measurements.*

The last parameter, what a dependence of the Cherenkov emission was observed on, is the toroidal magnetic field B_T. There were carried out measurements with the various magnetic field at low density and medium density at the fixed detector position (R_{ch}=70mm). The results of measurement are shown in tables 2.9 and 2.10. Dependences are shown in Fig 2.17.

B_T [T]	Number of shots (shot numbers)	$\Sigma U_{ch}t$ [V. ms]	σ [V.ms]
1.47	2 (#11,12)	712.5	125.8
1.36	1 (#13)	230.7	-
1.26	3 (#14,15,16)	222.5	103.5
1.12	2 (#17,18)	564.1	194.1
1.02	2 (#19,20)	885.8	378.1

Table 2.9: *B_T scan at medium density - electron side; shots #11-20*

B_T [T]	Number of shots (shot numbers)	$\Sigma U_{ch}t$ [V. ms]
1.46	1 (#32758)	409.9
1.41	1 (#32759)	475.6
1.33	1 (#32760)	680.3
1.41	1 (#32761)	482.6
1.36	1 (#32762)	603.5
1.25	1 (#32763)	1601.9
1.12	1 (#32764)	2059.1
1.01	1 (#32765)	2445.9
0.93	1 (#32766)	2439.5
0.86	1 (#32767)	2350.9

Table 2.10: *B_T scan at low density - electron side; shots #32758-32767*

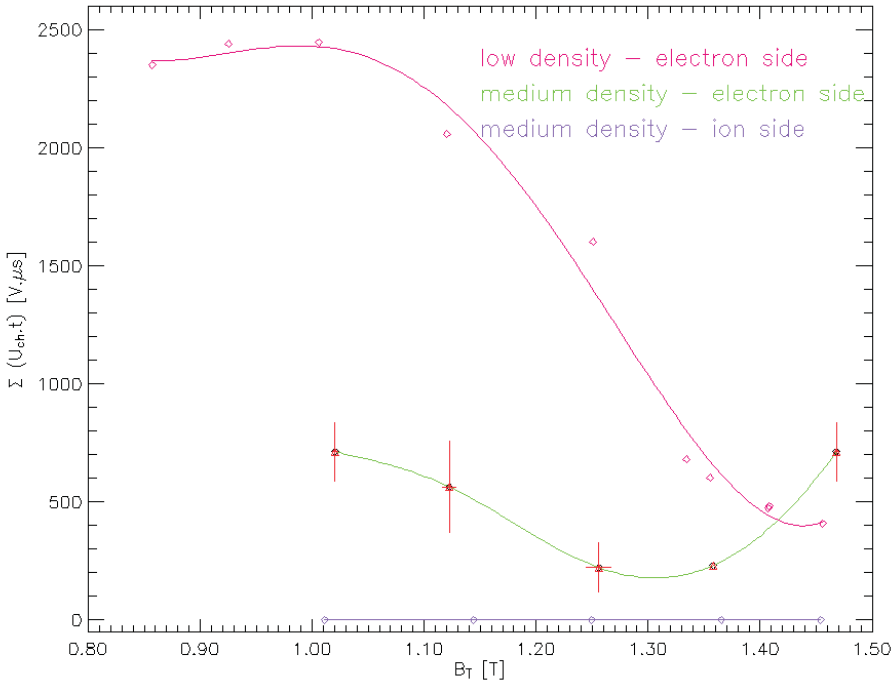

Figure 2.17: *Dependence of the Cherenkov emission on the toroidal magnetic field B_T measured for low density (red line), medium density (green line) and for side at medium density (purple line)*

A significant influence of the magnetic field change on particle confinement and consequently on the plasma density in tokamaks with no real-time density control, like in CASTOR, is observed. Therefore the Cherenkov emission at various magnetic field with variable position of the Cherenkov head was measured . Experimental data from these shots are presented in table 2.11 and Fig. 2.18. In Fig. 2.19 are shown details of dependence for particular values of Cherenkov detector position.

B_T [T]	R_{ch} [mm]	$\Sigma U_{ch}t$ [V. ms]	B_T [T]	R_{ch} [mm]	$\Sigma U_{ch}t$ [V. ms]
1.47	60	1570.9	1.45	75	23.9
1.47	60	1557.8	1.45	80	10.2
1.27	60	2171.5	1.45	80	11.9
1.27	60	2283.3	1.25	80	10.5
1.02	60	0.9	1.25	80	11.2
1.08	60	955.7	1.12	80	13.3
1.08	60	842.9	1.12	80	35.4
1.09	65	674.9	1.12	85	8.0
1.09	65	674.8	1.12	85	7.3
1.25	65	954.6	1.12	85	8.0
1.25	65	897.1	1.23	85	9.1
1.46	65	633.8	1.23	85	8.3
1.46	65	576.1	1.45	85	11.5
1.34	70	229.8	1.45	85	12.4
1.34	70	165.1	1.45	90	10.1
1.34	70	221.5	1.42	90	11.8
1.46	70	173.7	1.25	90	9.6
1.46	70	123.1	1.24	90	7.6
1.26	70	101.5	1.12	90	7.0
1.26	70	142.0	1.12	90	8.9
1.13	70	181.4	1.11	95	6.6
1.13	70	102.6	1.12	95	7.5
1.13	75	34.4	1.23	95	9.3
1.14	75	76.3	1.23	95	8.0
1.24	75	24.2	1.44	95	7.9
1.24	75	22.6	1.43	95	8.7
1.44	75	17.9	-	-	-

Table 2.11: *Combined B_T and position scan - electron side; shots #83-135*

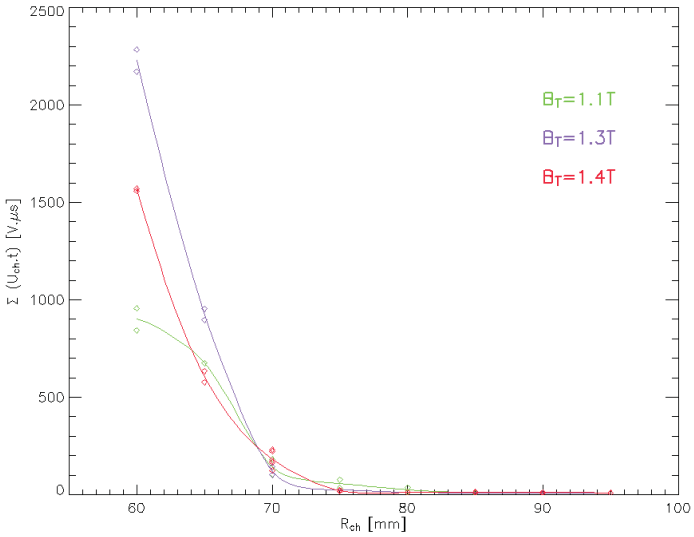

Figure 2.18: *Dependence of the Cherenkov emission on the position of the Cherenkov head for various toroidal magnetic field B_T measured for medium density*

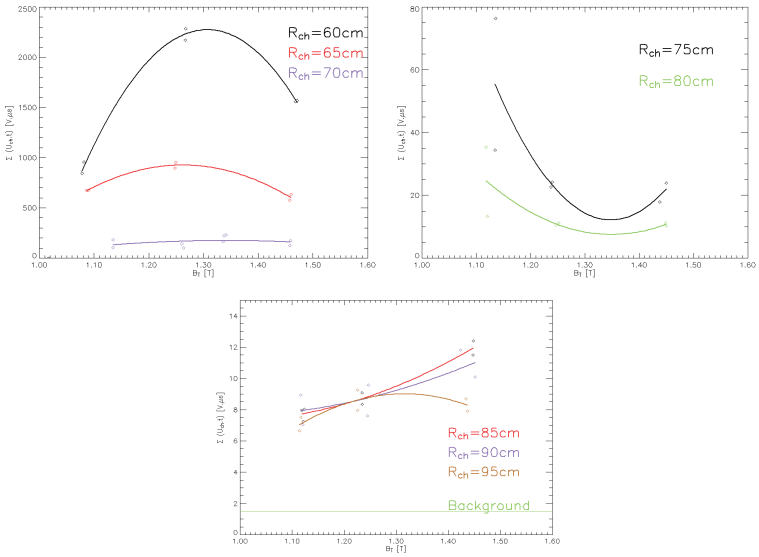

Figure 2.19: *Dependence of the Cherenkov emission on the position of the Cherenkov head for various toroidal magnetic field B_T measured for medium density. A background level is indicated by a green line on the bottom figure.*

Chapter 3

Discussion

In the previous sections it was shown that the measurements of fast electrons generated in discharges of the tokamak device using the Cherenkov radiation detector could be successfully realized. The described experimental set-up provided a sufficiently high gain and allowed a radial distribution of fast electrons to be measured. On the other hand, the use of the detector only inside the edge plasma region due to the thermal limit of the entrance window together with a presence of the parasitic signals originating namely in the direct radiation from the high-temperature tokamak plasma to the photomultiplier are the main constrains of the Cherenkov radiation-based systems.

A significant effort was spent to handle the parasitic signals, see section 2.5. As a result, properties of the direct radiation background from the tokamak were discovered. It was found experimentally the tree-lead brick bunker of the thickness 15 cm satisfactorily shields the photomultiplier that a standard deviation of the measured signal is typically less than few percents. A remarkable energy range in the direct radiation background was estimated using the different shielding of the photomultiplier. Appropriate energies using a lead shielding were estimated as E=(3.9±1.0)MeV, what gives the same range as a measurement using water shielding E=(3.8±0.1)MeV. Although it is clear that a real radiation spectrum from the tokamak is very wide, the inferred estimation of the dominating energy in a direct radiation background is still valid as a consequence of the form of the attenuation factor dependence on energy for lead Fig.2.10). The measured value of attenuation factor μ/ρ is situated in region of minimum of this dependence. Moreover, this construction is fortified by the same result for water shield-

ing, even if the dependence of the attenuation factor on energy for water is different than for lead. The origin of this radiation is still a puzzle and it will be subject for further investigations.

A protection of the detector head against interferences and the secondary radiation (e.g. Bremsstrahlung from the detector head shielding) was tested. The entrance window of the detector, by default oriented in the direction opposite to the plasma current allowing fast electron measurements, was turned around its axis by 180 degrees in agreement with the plasma current in some shots of the campaign. The recorded signals were in this case very low (practically negligible) as is shown in figures in chapter 2.

The experimental data obtained for a low-density plasma show a strong growth of the fast electron flux for the inner radial detector positions ($R_{ch} <$ 80 mm, Tab. 2.5 Fig 2.14). For plasma of medium density (above $10^{19}m^{-3}$, Tab. 2.4, Tab. 2.6, Fig. 2.13 and Fig. 2.14) the electron flux is considerably lower, mainly for R_{ch}=60-80mm, but the character of dependences is very simillar. Concluding, the Cherenkov signal depends very strongly on the vertical observation radius (R_{ch}), i.e. the emission clearly increases going deep into a plasma, what is a behavior similar for a wide range of plasma densities (n_e).

A next considerable effect concerning the signal evolution is caused by the plasma density. In high-density discharges, an initiatory increase of the Cherenkov signal is followed by a stationary phase. It can be interpreted as a constant production and loss rate of the fast electrons. On the other hand, low-density discharges show almost an exponential growth of the Cherenkov signals from the time given by the observed radius till the end of the discharge. Such effect should be connected with a reaching of the critical energy in low-density discharges.

In Fig. 2.14 one can see that the Cherenkov signal is greater for a low plasma density than for medium. It can be explained by the help of that the plasma density substantially affects a plasma thermalization, i.e. collisionality is lower for lower densities. For densities greater than $12 * 10^{18}m^{-3}$ probably a worse plasma column position stabilization causes an increase of the fast electron flux. However, it should be remarked that the time of the initiatory increase of the Cherenkov emission remains nearly the same for the whole range of densities, if the detector position is fixed. For typical CASTOR discharges featuring by the averaged plasma densities equal to $8 - 12 * 10^{18}m^{-3}$, the fast electron fluence reaches its minimum level, see Fig.2.7.

At the same plasma conditions, a number of fast electrons should be proportional to the plasma current representing their source, see Fig.2.16 One can observe that the electron beam intensity increases with the plasma current, Fig.2.16. The big jitter of the experimental points might be explained by considerable differences in plasma densities during different discharges. We have to consider also that here is no real time density control on CASTOR and due to there can be also different plasma profiles For a better interpretation it will be necessary a next investigation.

The dependence of the Cherenkov signal on the toroidal magnetic field derived from the shots with the different values of the plasma density is presented in Fig.2.17. For low densities the Cherenkov signal increases with decreasing magnetic field. The same dependence for medium densities cannot be simply interpreted due to a big scatter of experimental points.

In Fig.2.18 a comparison of the dependence of the Cherenekov signal on the radial position at diferent values of B_T is shown. This plot again confirms that the Cherenkov signal depends very strongly on the vertical observation radius (R_{ch}) as it was shown before.

According to an analysis of the Langmuir probe data [11] and Fig.2.19 it seems that the fast electron generation is influenced by changes of the toroidal magnetic field differently in the confined plasma region (R_{ch} <70 mm), in the region with a long connection length to the limiter (70mm< R_{ch} <85mm) and in the limiter shadow (R_{ch} >85mm). A character of the dependeces in Fig 2.19 suggests that near radius R_{ch}=70mm the last closed flux surface (LCFS) is situated, what was fully confirmed by probe measurements.

Chapter 4

Conclusion

The most important results of this thesis can be interpreted as follows. The changes of the Cherenkov detetor system allowed a reduction of electromagnetic interferences and a direct hard radiation was eliminated completely. It was verified that the recorded Cherenkov signals originates only by fast electrons (>50keV). On the CASTOR tokamak, the dependences of the fast electron signals on the radial position of the Cherenkov detector, as well as on the plasma density, plasma current and toroidal magnetic field value were investigated and explained.

A question on an unclear origin of the hard radiation of energy approximately 3.9MeV reaching the shielded detection system only during the tokamak discharges stays still unanswered.

It can be concluded that appropriate Cherenkov detectors might be applied for investigation of fast electrons in tokamak-type facilities. However, real experimental conditions and in particular thermal limitations during high-current discharges must be taken into a consideration.

This thesis is occupied by a part of result obtained from measurement, which were carried out on tokamak CASTOR. The results of the statistical approach using a single-count analysis of the time-resolved Cherenkov data indicates possible transport mechanisms of fast electrons - the fast burst losses in combination with a slow diffusion.

Bibliography

[1] Wesson J.: *Tokamaks*, Caledon Press, Oxford, 1997

[2] Mlynář J.: *Analýza tvrdého rentgenovského záření na zařízení tokamak CASTOR*, diplomová práce, MFF UK, Praha, 1991

[3] Ďuran I.: *Runaway electrons in tokamaks*, ročníková práce, FJFI ČVUT, Praha, 1995

[4] Andersson F.: *Runaway Electrons in Tokamak Plasmas*, diploma thesis, Chalmers University of Technology, Goeteborg, 2003

[5] Knoepfel H., Spong D.A.: *Runaway electrons in toroidal discharges*, Nuclear Fusion 19 (1979), No.6, pp. 785-826, 1979

[6] Jaspers R.: *Diagnostic to measure the infrared synchrotron radiation from relativistic runaway electrons*, Diagnostic for Contemporary Fusion Experiments, Varenna (Bologna), 1991

[7] Jaspers R.: *Experimental investigation of runaway electron generation in Textor*, Nucl. Fus. 33 (1993), No.12,1775, 1993

[8] Jaspers R.: *Islands of Runaway Electrons in the Textor Tokamak and Relation to Transport in a Stochastic Field*, Phys.Rev.Lett., FOM 19.5.1994, 1994

[9] Jaspers R.: *Confinement of Relativistic Electrons in Textor*, ISPP-14 (Varenna 1993), Local Transport Studies in Fusion Plasmas, p.193, 1993

[10] Finken K.H.: *Observation of infrared synchrotron radiation from tokamak runaway electrons in Textor*, Nucl.Fus., Vol.30,No.5 (1990), p.859-869

[11] Jakubowski L., Sadowski M.J., Stanislawski J., Malinowski K., Zebrowski J., Weinzettl V., Stockel J., Vácha M., Peterka M.: *Design and tests of Cherenkov detector for measurements of fast electrons within CASTOR tokamak*, 34th EPS Conference on Plasma Physics, Warsaw, Poland, 2/7-6/7/2007

[12] Jakubowski L., Stanislawski J., Sadowski M.J., Zebrowski J., Weinzettl V., Stöckel J.: *Design and tests of Cherenkov detector for measurements of fast electrons within CASTOR tokamak*, Czech.J.Phys., Vol.56(2006), Suppl. B, pp. 98-103, 2006

[13] Dereniak F.I., Crowe D.G.: *Optical Radiation Detectors*, John Wiley & Sons, USA, 1984

[14] Weinzettl V.: *Prostorové a časové chování lehkých nečistot ve vysokoteplotním plazmatu tokamaku CASTOR*, disertační práce, KFE FJFI ČVUT, Praha, 2005

[15] Tkachenko N.V., *Optical Spectroscopy, Methods and Instrumentations*,Elsevier, 2006

[16] Hubbell J.H. and Seltzer S.M.: *Tables of X-Ray Mass Attenuation Coefficients and Mass Energy-Absorption Coefficients (version 1.4) [Online]*, National Institute of Standards and Technology, Gaithersburg, 2004